

## Article

# Measurement of Dilational Modulus of an Adsorbed BSA Film Using Pendant Bubble Tensiometry: From a Clean Interface to Saturation

Siam Hussain <sup>1</sup>, Johann Eduardo Maradiaga Rivas <sup>1</sup>, Wen-Chi Tseng <sup>1</sup>, Ruey-Yug Tsay <sup>2</sup>, Boris Noskov <sup>3</sup> and Giuseppe Loglio <sup>4</sup> and Shi-Yow Lin <sup>1,\*</sup>

<sup>1</sup> Department of Chemical Engineering, National Taiwan University of Science and Technology, 43, Sec. 4, Keelung Road, Taipei 106, Taiwan; siam.hussain95@gmail.com (S.H.); maradiaga.johann@gmail.com (J.E.M.R.); tsengwc@mail.ntust.edu.tw (W.-C.T.)

<sup>2</sup> Department of Biomedical Engineering, National Yang-Ming Chiao Tung University, 155, Sec. 2, Linong St., Taipei 112, Taiwan; ycutsay@nycu.edu.tw

<sup>3</sup> Department of Colloid Chemistry, St. Petersburg State University, Universitetsky pr. 26, 198504 Saint Petersburg, Russia; b.noskov@spbu.ru

<sup>4</sup> Italian National Research Council—CNR, Institute of Condensed Matter Chemistry and Technologies for Energy, 16149 Genoa, Italy; giuseppe.loglio@ge.icmate.cnr.it

\* Correspondence: sylin@mail.ntust.edu.tw; Tel.: +886-2-2737-6648

**Abstract:** Two open issues on the measurement of the dilational modulus ( $E$ ) for an adsorbed protein film during the adsorption process have been unacknowledged: how  $E$  varies during the adsorption and the length of time needed to attain a stable  $E$  value. A new approach for detecting the  $E$  variation from a clean air–water interface to saturated film and estimating the time needed to reach a saturated state was proposed. A pendant bubble tensiometer was utilized for measuring the relaxations of surface tension (ST) and surface area (SA), and the  $E$  was evaluated from the relaxation data of minute distinct perturbances. The data showed a clear variation in  $E$  during the BSA adsorption:  $E$  sharply decreased to a minimum at the early stage of BSA adsorption; then, it rose from this minimum and oscillated for a while before reaching an  $E$  corresponding to a saturated BSA film after a significant duration. The adsorbed BSA film took ~35 h to reach its saturated state, which was much longer than the reported lifetime of the adsorbed film in the literature. A rapid surface perturbation (forced bubble expansion/compression) could change the  $E$ , causing a significant drop in  $E$  followed by a slow increase to the original stable value.

**Keywords:** dilational modulus; bovine serum albumin; adsorbed film; pendant bubble tensiometry; perturbed interface; interfacial rheology

**Citation:** Hussain, S.; Rivas, J.E.M.; Tseng, W.-C.; Tsay, R.-Y.; Noskov, B.; Loglio, G.; Lin, S.-Y. Measurement of Dilational Modulus of an Adsorbed BSA Film Using Pendant Bubble Tensiometry: From a Clean Interface to Saturation. *Colloids Interfaces* **2024**, *8*, 4. <https://doi.org/10.3390/colloids8010004>

Academic Editor: Eduardo Guzmán

Received: 31 October 2023

Revised: 19 December 2023

Accepted: 21 December 2023

Published: 22 December 2023



**Copyright:** © 2023 by the authors. Licensee MDPI, Basel, Switzerland. This article is an open access article distributed under the terms and conditions of the Creative Commons Attribution (CC BY) license (<https://creativecommons.org/licenses/by/4.0/>).

## 1. Introduction

Protein films at an air–water interface have garnered considerable attention due to their potential applications in various industrial and scientific fields. These films exhibit remarkable biocompatibility and adaptability, making them suitable for use as biomedical scaffolds [1,2], biodegradable packaging [3–5], supramolecular assemblies [6,7], biosensors [8,9], colloidal stabilizer [10–12], and catalysts [13].

This widespread applicability has led to a growing interest in investigating the physicochemical and rheological properties of protein films, as these properties notably influence industrial operations. In general, the findings from the relevant literature (e.g., ref. [14–20]) have revealed that the physicochemical, rheological, and structural properties of protein films at an air–water interface are primarily influenced by the intrinsic stability of the protein molecule (ability to maintain the native folded conformation and resist

unfolding or aggregation), amino acid composition, molecular conformation, and solvent pH and ionic strength.

In addition, ref. [14–20] consistently reported that forming a stable/saturated film required significant time. For instance, Dickinson et al. [15] observed that the steady-state shear stress ( $\sigma_{ss}$ ) for a  $\beta$ -lactoglobulin (BLG) film was not attained even after 80 h of equilibration, while Varvara et al. [16] reported that the steady-state shear viscosity ( $\mu_s$ ) was attained only after 20–30 h. Moreover, studies using spectroscopy-based techniques [14,16,17,20] consistently reported that the slow conformational changes and network formation among adsorbed molecules contribute to the significant time requirement. Strazdaite et al. [20] and Postel et al. [17] both observed continual changes in the intensity of IRRAS spectra and X-ray reflectivity, respectively, over 24 h (since the film began to form), further supporting this time issue. These findings are detailed in Table S1 of the Supplementary Material for the reader's convenience.

However, the significant time needed for obtaining stable shear properties ( $\sigma_{ss}$  and  $\mu_s$ ) of adsorbed protein film does raise concerns regarding the measurement of interfacial rheological parameters like dilational modulus ( $E$ ), which is a parameter controlling the functionality and stability of protein films [21,22]. These concerns included the following: (i) What was the state of the adsorbed film when  $E$  was measured? Was it a saturated film? (ii) How does  $E$  vary during the progressive adsorption of a protein film? (iii) How long does it take for a protein film to obtain a stable  $E$  value for a saturated film?

A literature review, comparing the experimental conditions of studies investigating the dilational rheology of globular protein films (BSA, BLG, ovalbumin (OVA), lysozyme (LYS), human serum albumin (HSA); Table S2a–e), revealed significant variations in the film's lifetime when  $E$  was measured. Despite this variation, the measurement duration (lifetime of protein film,  $t_{life}$ ) could be roughly classified: (i)  $t \sim 24$  h, (ii)  $t = 3$ –6, (iii)  $t = 1$ –3, and (iv)  $t \leq 1$  h, as shown in Table S3. The large variation in  $t_{life}$  likely indicated that the reported  $E$  values might correspond to different states of the adsorbed film but not that of a saturated film, particularly those  $E$  measured at short  $t_{life}$ . Note that there is no answer in the literature on how long it takes for an adsorbed film to reach its saturated state.

In light of these concerns, this work studied the variation in  $E$  of an adsorbed protein film, from a clean air–water interface to a saturated film, and assessed the time needed for the adsorbed film to reach its saturated state. BSA was the model protein, and the dilational modulus of an adsorbed BSA film was evaluated throughout its adsorption by monitoring the relaxations of surface tension (ST) and surface area (SA) of a pendant bubble. The data showed that the  $E$  of an adsorbed BSA film exhibited a clear variation during the adsorption process, reaching a minimum at the early stage and then rising and oscillating before reaching a stable value after a considerable time period.

## 2. Materials and Methods

**Material.** Bovine serum albumin (lyophilized powder, purity  $\sim 99.0\%$ , essentially globulin free, molecular weight = 66.4 kD) was purchased from Sigma-Aldrich (St Louis, MO, USA) and utilized in its original form. Ultrapure water (specific conductance  $\kappa < 0.057$   $\mu\text{S}/\text{cm}$ , obtained using the UP-DQ Plus System (Pure Yes Ltd., Taipei, Taiwan)) was used for preparing the protein solutions. The glassware and ultrapure water used for preparing the protein solutions were autoclaved for two hours to reduce the risk of microbial contamination. The cell was cleansed by first being immersed in a strongly acidic solution, then in dilute HCl, and rinsed with ultrapure water after each immersion. Furthermore, the quartz cell (containing the BSA solution) was nearly covered during the ST measurement.

**Solution preparation.** The BSA solutions were prepared only with ultrapure water (i.e., without an aqueous buffer such as sodium phosphate or phosphate buffer saline). Firstly, a weighed quantity of BSA was added to a volumetric flask, which was followed by the addition of sterilized ultrapure water. The resulting mixture was stirred at room temperature for  $\sim 2$  h. Once the solution was mixed well, the flask was transferred to a

thermostatic bath ( $T = 25\text{ }^{\circ}\text{C}$ ) and kept there for  $\sim 1$  hr. A fixed amount ( $\sim 28\text{ mm}^3$ ) of this BSA solution was poured into the quartz cell ( $22 \times 42 \times 44\text{ mm}$ ) for ST measurement.

**Tensiometer.** A video-enhanced pendant bubble tensiometer was utilized for measuring the relaxations of surface tension (ST) and surface area (SA) of a purely aqueous BSA solution and the pendant bubble (at  $T = 25\text{ }^{\circ}\text{C}$ ); details of its working methodology are in ref. [23,24]. Once the BSA solution was poured into a quartz cell and placed on the adjustable stage, it was kept still for  $\sim 30$  min to approach a static state. Then, a pendant air bubble (diameter of  $\sim 2\text{ mm}$ ) was formed at the center of the solution in  $\sim 2\text{ s}$  with an inverted stainless-steel needle (18-gauge, O.D = 1.27 mm, I.D = 0.84 mm). Sequential images of the bubble were taken and then processed to determine the edge coordinates, which were then fitted with the Young–Laplace equation to determine the ST and bubble SA. The ST and SA relaxations were measured at  $C = 0.4\text{--}15\text{ (}10^{-10}\text{ mol/cm}^3\text{)}$ . Note that (i) the reproducibility of the ST measurements was ca. 0.1 mN/m [25] and (ii) during the latter stage of the adsorption process, some perturbations (rapid compression–expansion of the pendant bubble) were conducted to verify if the ST relaxed back to its previous value. Further, the quartz cell was kept nearly covered during the ST measurement to mitigate evaporation and its potential impact on bulk concentration.

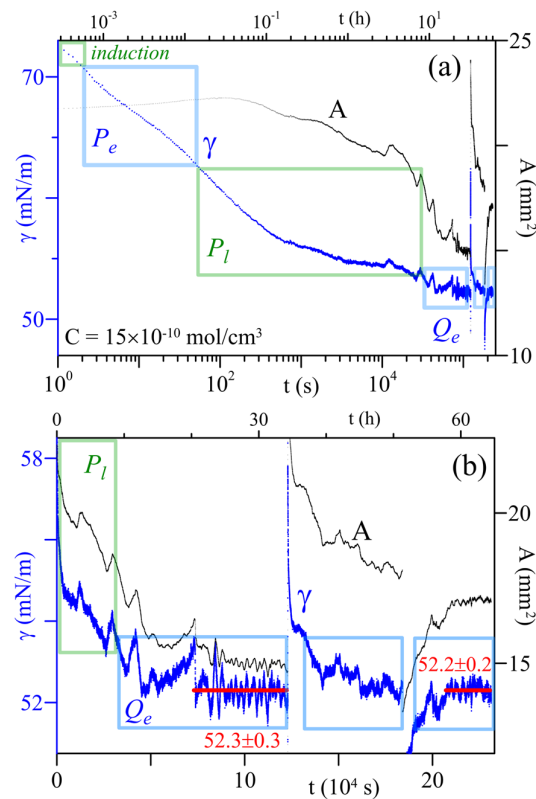
**Surface perturbation.** A pendant bubble was formed on the tip of a stainless-steel inverted needle, which, in turn, was connected to a normally closed port of a three-way miniature solenoid valve via 1/16 in. (1.6 mm) ID Teflon tubing (placed inside the thermostatic chamber). During the ST measurement, the ‘air inside the pendant bubble and Teflon tubing (between the valve and needle)’ formed a closed system. The temperature outside the chamber was maintained at  $25.0^{\circ}1 \pm \text{C}$ . The temperature inside the chamber ( $T_s$  and  $T_{\text{air}}$ ) varied with time, which likely caused the bubble volume and bubble SA to fluctuate by a few percent.

**Dilational modulus.** The dilational modulus was evaluated following the manner in ref [26]. The distinct perturbances (minute compression/expansion of the bubble surface, ( $\Delta A = 0.05\text{--}0.8\text{ mm}^2$ ;  $A_0 = 15\text{--}22\text{ mm}^2$ )) were first identified amidst the overall ST and SA relaxations. These perturbances were distinguishable by a nearly linear and well-defined change in SA ( $\Delta A > \sim 0.05\text{ mm}^2$ ) and ST ( $\Delta\gamma > \sim 0.1\text{ mN/m}$ ). Each distinct perturbation was examined: (i) the onset and the end were located; (ii) a linear fit was applied to the ST and SA relaxation data of the perturbation; (iii) the dilational modulus,  $E_i = (d\gamma/dt)/(d\ln A/dt)$ , was calculated as the ratio of the rate of ST change ( $d\gamma/dt$ ) to the relative surface expansion rate ( $d\ln A/dt$ ). In addition, the average dilational modulus ( $E_{\text{avg}}$ ) of several perturbances was obtained from the slope of the best-fitting line ( $d\gamma/dt$  vs.  $d\ln A/dt$ ).

### 3. Results

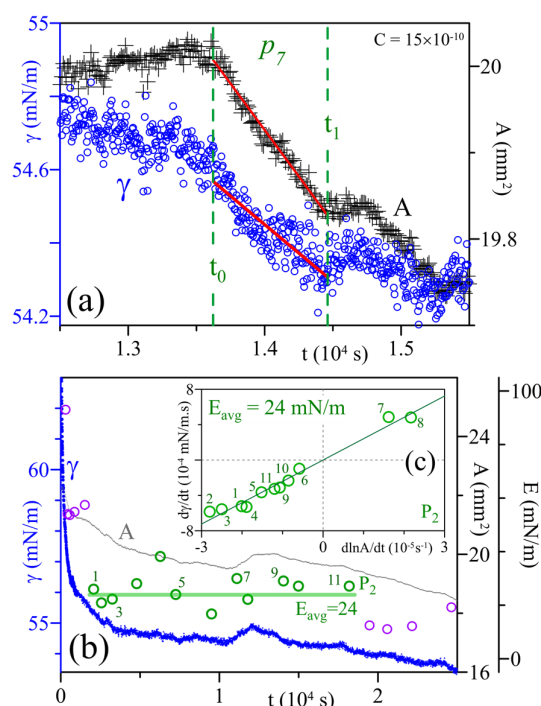
The dynamic ST of a BSA<sub>(aq)</sub> solution at  $C_{\text{BSA}} = 0.4\text{--}15\text{ (}10^{-10}\text{ mol/cm}^3\text{)}$  was measured at  $25\text{ }^{\circ}\text{C}$  using a pendant bubble tensiometer, starting from a clean air–water interface to a saturated adsorbed film. The dilational modulus of the adsorbed BSA film was evaluated during the whole adsorption process. Tiny perturbances were identified and analyzed to evaluate the dilational modulus,  $E = (d\gamma/dt)/(d\ln A/dt)$ .

Figure 1 illustrates the relaxations of ST and SA for  $C_{\text{BSA}} = 15 \times 10^{-10}\text{ mol/cm}^3$ . During the first few hours, the ST exhibited a relatively smooth and gradual decrease (from 72 mN/m): at  $t < \sim 0.5\text{ h}$ , the SA remained somewhat constant ( $\pm 1.5\%$  variation); then, it decreased steadily (Figure 1a) at  $t < \sim 10\text{ h}$ . Afterward, at  $t > \sim 10\text{ h}$ , the ST relaxed slowly; then, it eventually reached and remained essentially constant (at  $\sim 52.2\text{ mN/m}$ ) while exhibiting prominent and sustained fluctuations (Figure 1b). These ST fluctuations were generally observed to be in harmony with the minute variations in SA (Figure S1 of the Supplementary Material). Note that the ST relaxation of BSA solution can be generally divided into three distinct regimes [27]: induction, post-induction (early ( $P_e$ ), latter ( $P_l$ )), and quasi-equilibrium ( $Q_e$ ), as shown in Figure 1 and further illustrated in Figure S2 for  $C_{\text{BSA}} = 0.4$  and  $6\text{ (}10^{-10}\text{ mol/cm}^3\text{)}$ .



**Figure 1.** Surface tension ( $\gamma$ ) and surface area ( $A$ ) relaxations of a purely aqueous BSA solution and the pendant bubble at  $C = 15 \times 10^{-10} \text{ mol/cm}^3$ ; presented in (a) log and (b) linear time scales.  $P_e$ ,  $P_l$ , and  $Q_e$  indicate post-induction (early, latter) and quasi-equilibrium regimes, respectively.

In general, more than 300 perturbances were identified amidst the overall SA and ST relaxations of each run. More than half of these perturbances were distinct (i.e.,  $\Delta A > \sim 0.05 \text{ mm}^2$  and  $\Delta \gamma > \sim 0.1 \text{ mN/m}$ ) and characterized by nearly linear changes in SA and ST, as illustrated by examples in Figures 2a, S3 and S4.



**Figure 2.** (a) Relaxations of ST ( $\gamma$ ) and SA ( $A$ ) at  $C_{BSA} = 15 \times 10^{-10}$  mol/cm<sup>3</sup>, depicting a perturbation identified at the  $P_i$  regime. (b) Variation of the dilational modulus ( $E_i$ ,  $\circ$ ) of the BSA film as a function of time alongside the corresponding ST and SA relaxations. (c) Dependency between the rate of ST change ( $d\gamma/dt$ ) and relative surface expansion rate ( $d\ln A/dt$ ) of those perturbances ( $\circ$ ) identified at  $t = 0.2\text{--}1.8$  ( $10^4$  s), wherein  $E_{avg}$  was obtained from the slope of the best-fitted line (marked in red).

The dilational modulus ( $E_i$  and  $E_{avg}$ ) was evaluated following the manner in ref. [26]. Briefly, the onset (at  $t_0$ ) and end ( $t_1$ ) of each perturbation were first identified (indicated by vertical dashed lines in Figures 2a, S3, and S4). As the ST and SA relaxed in a nearly linear manner during the perturbation, the relaxation data were best fitted linearly to obtain  $d\gamma/dt$  and  $d\ln A/dt$ ; then, a local dilational modulus ( $E_i = (d\gamma/dt)/(d\ln A/dt)$ ) was estimated. The data ( $t_0$ ,  $t_1$ ,  $A_0$ ,  $A_1$ ,  $\gamma_0$ ,  $\gamma_1$ ,  $d\ln A/dt$ ,  $d\gamma/dt$ , and  $E_i$ ) corresponding to perturbation  $p_7$  were tabulated in Table S5.

Using this approach, the local dilational modulus ( $E_i$ ) at a specific short region of time ( $t_i$ ) was evaluated for numerous (150–200) distinct perturbances on each run (denoted by circles in Figure 2b). Alternatively, the data,  $d\gamma/dt$  and  $d\ln A/dt$ , of several distinct perturbances, identified successively over a considerably long time range ( $t = 0.2\text{--}1.8$  ( $10^4$  s)), were plotted in a  $d\gamma/dt$  vs.  $d\ln A/dt$  plot (circles in Figure 2c). These data points were then best fitted linearly (through the origin) to obtain the  $E_{avg}$  (the slope of this best-fitting line) over this time interval; the horizontal line in Figure 2b shows this  $E_{avg}$ .

The  $E_{avg}$  at other time intervals was obtained similarly, as illustrated by the examples at  $t = 0.04\text{--}0.15$  ( $10^4$  s) and  $9.3\text{--}10.5$  ( $10^4$  s) in Figure S5. When these values of  $E_{avg}$  were plotted alongside the ST and SA relaxations, as shown in Figure 3 (and Figure S6), a clear variation in  $E_{avg}$  was observed during the BSA adsorption process. The data in Figure 3 indicate that initially,  $E_{avg}$  sharply decreased (from  $\sim 90$  mN/m, green  $\square$ ) and reached a minimum of  $\sim 16$  mN/m (red  $\Delta$ ) at the  $P_i$  regime (red  $\circ$ ). Afterward, at the  $Q_e$  regime (blue and purple  $\circ$ ),  $E_{avg}$  rose from this minimum, oscillated at  $\sim 30$  mN/m ( $+$ ) for a considerable duration, and eventually reached a relatively stable value of  $\sim 40$  mN/m (green circles). This relatively stable  $E_{avg}$  indicates that it takes a considerably long time ( $>10^5$  s) for the adsorbed BSA molecules to form a saturated film even though the ST had reached its equilibrium value a long time ago.

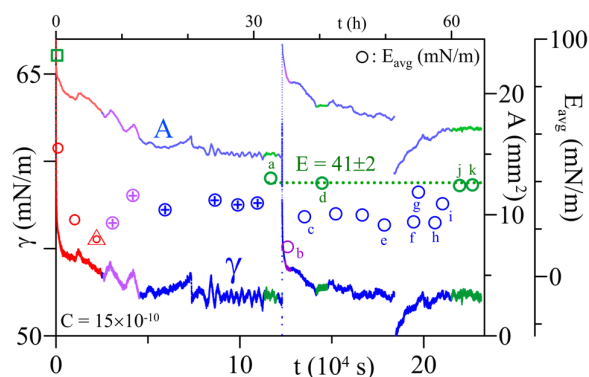


**Figure 3.** Variation of  $E_{avg}$  (average dilational modulus) of the adsorbed BSA film as a function of time alongside the corresponding ST ( $\gamma$ ) and SA ( $A$ ) relaxations at  $C_{BSA} = 15 \times 10^{-10}$  mol/cm<sup>3</sup>. The triangle ( $\Delta$ ) signifies the minimum value of  $E_{avg}$  and the plus (+) signifies the subsequent increase and oscillation.

A similar variation in  $E_{avg}$ , during the BSA adsorption, was also observed at other BSA concentrations. Figure 4 (and Figure S7) shows another two examples at  $C_{BSA} = 0.4$  and  $6$  ( $10^{-10}$  mol/cm<sup>3</sup>):  $E_{avg}$  dropped sharply from  $\sim 125$  mN/m, reached a minimum (15 and 17 mN/m, respectively;  $\Delta$ ), rose, oscillated for a considerable time (+), and then reached a stable  $E_{avg}$  after a significant duration (green ○) at  $t > 10^5$  s.

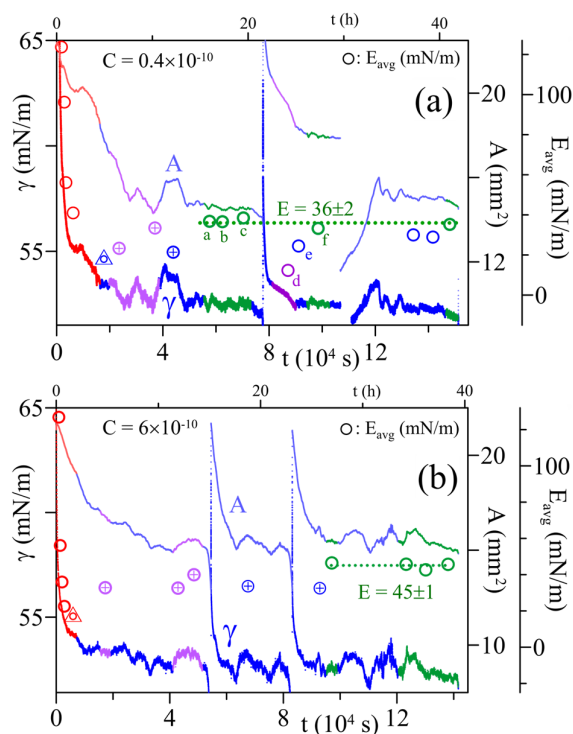


**Figure 4.** Variation of  $E_{avg}$  (○) of the adsorbed BSA film as a function of time alongside the corresponding ST ( $\gamma$ ) and SA ( $A$ ) relaxations at  $C_{BSA} = 0.4$  (a) and  $6.0$  (b) ( $10^{-10}$  mol/cm<sup>3</sup>).

There is limited available information in the literature on the time needed for an adsorbed film to reach its saturated state. How long did it take for an adsorbed BSA film to reach its saturated state? The time needed to reach saturation ( $t_{sat}$ ) was estimated from the variation in  $E_{avg}$  at  $C_{BSA} = 0.05$ – $60$  ( $10^{-10}$  mol/cm<sup>3</sup>) (Figures 3 and 4): (i) the earliest stable  $E_{avg}$  detected, corresponding to a saturated adsorbed film, was identified and (ii) the ST and SA relaxations within the time interval covered by this  $E_{avg}$  was examined. The  $t_{sat} = 27$ – $40$

h (9.7–14.5 ( $10^4$  s), averaging at  $\sim 35$  h) (shown in Figure S8). This  $t_{\text{sat}}$  is much longer than the film's lifetime ( $t_{\text{life}}$ ) in the literature for BSA (0.05–24 h, Table S2b), thus suggesting that the reported  $E$  values were likely not that of a saturated film.

The  $t_{\text{sat}}$  was also compared to the time needed to reach the equilibrium ST. Figure S9 illustrates an example at  $C_{\text{BSA}} = 15 \times 10^{-10}$  mol/cm<sup>3</sup>: the equilibrium ST was reached in  $\sim 21$  h, which was much shorter than the  $t_{\text{sat}}$  ( $\sim 32$  h). This likely suggested that despite reaching the equilibrium ST, an adsorbed BSA film might require a longer time to rearrange in order to reach its saturated state. However, further study is needed for confirmation.

At the  $Q_e$  (quasi-equilibrium) regime, some large, forced perturbations (rapid compression/expansion of the pendant bubble) were conducted to (i) verify if the ST relaxed back to its previous value and (ii) evaluate how  $E_{\text{avg}}$  would be affected by such rapid surface perturbations. Figure 5 illustrates an example at  $C = 15 \times 10^{-10}$  mol/cm<sup>3</sup>: when the pendant bubble was subjected to a forced perturbation (initial  $\sim 25\%$  SA decrease in  $\sim 0.7$  s, then abrupt 116% increase in  $\sim 5$  s; detailed in Figure S10),  $E_{\text{avg}}$  sharply dropped from  $\sim 40$  (of a saturated film) to  $\sim 13$  mN/m; then, it rose continually, approached and reached the previous  $\sim 40$  mN/m. A similar tendency was also observed when the pendant bubble was rapidly perturbed at  $C_{\text{BSA}} = 0.4 \times 10^{-10}$  mol/cm<sup>3</sup> (Figures S11 and S12). This considerable decrease and the subsequent slow increase in  $E_{\text{avg}}$  may indicate a breakage [28,29] and recovery [30,31] of the adsorbed BSA film.

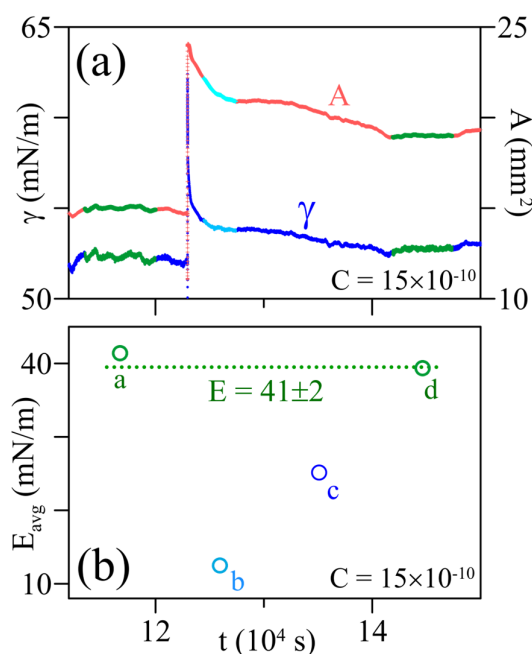


**Figure 5.** (a) Relaxations of ST ( $\gamma$ ) and SA ( $A$ ) at  $C_{\text{BSA}} = 15 \times 10^{-10}$  mol/cm<sup>3</sup>, during a rapid perturbation (compression–expansion) of the pendant bubble and (b) the corresponding variation of  $E_{\text{avg}}$  (○) of the adsorbed BSA film as a function of time. The labels 'a–d' signifies the  $E_{\text{avg}}$  values in Figure 3.

#### 4. Discussion

The first few perturbances (characterized by a somewhat synchronized change in ST and SA) were generally identified at the  $P_I$  (latter post-induction) regime (e.g.,  $t = 130$ – $330$  s at  $C_{\text{BSA}} = 15 \times 10^{-10}$  mol/cm<sup>3</sup>, Figure S13). The  $E_{\text{avg}}$  obtained from these first few perturbances (with a poor fit,  $E_{\text{avg}} = 173$  mN/m for perturbances ①–③, Figure S14 and Table S5) were much larger than those for a saturated BSA film ( $E_{\text{avg}} = 41$  mN/m); the significantly higher  $E_{\text{avg}}$  was likely not real but rather due to the significant contribution of BSA adsorption (which caused a significant decrease in ST) during the  $P_I$  regime, and hence, the  $E_{\text{avg}}$  of perturbances ① and ② was not used in Figure 3. Note that the reliability of the  $E_{\text{avg}}$

values reported at later instances of the  $P_l$  and  $Q_e$  regime (e.g.,  $P_{1-3}$  in Figure S15) are much higher because (i) they were obtained from the data of multiple perturbances and (ii) a good linear relationship was observed on  $d\gamma/dt$  vs.  $d\ln A/dt$ . Similar behavior was also observed at other  $C_{BSA}$ : an additional example at  $C_{BSA} = 6 \times 10^{-10}$  mol/cm<sup>3</sup> is shown in Figure S16 of the Supplementary Material.

Differing behaviors were reported in several studies, investigating the desorption of proteins from the air–water interface (using radioactive tracer [32–34] and spectroscopy-based methods [35–37]). For instance, lysozyme [32] and  $\beta$ -casein [34] were reported to desorb under specific conditions, but phosvitin [36] and gliadins [35] did not. Recently, BSA ( $C = 0.3 \times 10^{-10}$  mol/cm<sup>3</sup>) was reported to desorb out of an adsorbed air–water interface by using rapid pendant bubble compression [38]. Figure 6 illustrates similar evidence for BSA desorption (after bubble compression) at  $C_{BSA} = 0.4 \times 10^{-10}$  mol/cm<sup>3</sup>: the SA decrease  $\sim 35\%$  in  $\sim 5$  s caused the ST to decrease from  $\sim 52$  to  $\sim 45$  mN/m (where the adsorbed BSA film was likely at an overcrowded state).

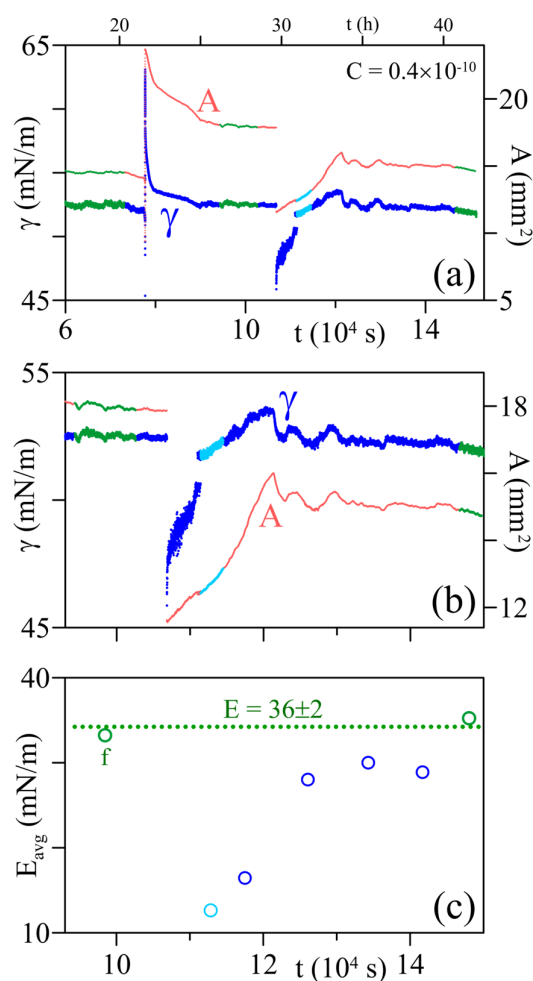


**Figure 6.** (a) Relaxations of ST ( $\gamma$ ) and SA ( $A$ ) at  $C_{BSA} = 15 \times 10^{-10}$  mol/cm<sup>3</sup>, during a rapid perturbation (compression–expansion) of the pendant bubble and (b) the corresponding variation of  $E_{avg}$  of the adsorbed BSA film as a function of time. The labels ‘a–d’ signifies the  $E_{avg}$  values in Figure 3.

The results of this study reveal a notable disparity between the time required for an adsorbed protein film to reach saturation and the time necessary to achieve equilibrium surface tension (ST). Specifically, despite reaching equilibrium ST, an adsorbed BSA film may necessitate an extended duration to rearrange and achieve a stable saturated state. A parallel examination of the literature data on high molecular weight compounds,



exemplified by block copolymers like PEO-PPO variants [39–41], discloses equilibration times ranging from 15 to 50 h, which are contingent on concentration. This parallels our findings, indicating a potential trend for other high molecular weight compounds: the time needed for the adsorbed film to attain a stable saturated state could surpass its equilibration time. This observation prompts further consideration in future studies, emphasizing the need for in-depth research to substantiate and explore this behavior across various compounds.

## 5. Conclusions

In this study, the relaxations of ST ( $C_{BSA} = 0.4\text{--}15$  ( $10^{-10}$  mol/cm<sup>3</sup>), purely aq. solution) and bubble SA were measured using a pendant bubble tensiometer throughout the BSA adsorption process: moving from an initially clean air–water interface to a saturated state. The  $E_i/E_{avg}$  of the adsorbed BSA film was then evaluated from the relaxation ST and SA data of minute distinct perturbances. Irrespective of the  $C_{BSA}$ , a clear variation in  $E_{avg}$  was observed during the BSA adsorption:  $E_{avg}$  significantly decreased to a minimum at an early stage of the BSA adsorption; then, it rose from this minimum and oscillated for a while before reaching a  $E_{avg}$  of a saturated BSA film after a significant time period of ~35 h. In addition, the  $E_{avg}$  of a saturated BSA film was notably influenced by rapid surface perturbations: there was a significant drop in  $E_{avg}$  followed by a slow increase back to the original stable  $E_{avg}$  value.

**Supplementary Materials:** The following supporting information can be downloaded at <https://www.mdpi.com/article/10.3390/colloids8010004/s1>, Table S1. A literature review—key findings in studies investigating the physicochemical and rheological properties of protein films at an air–water interface. Table S2a. A comparison of the experimental conditions in studies investigating the dilational rheology of adsorbed BLG films at an air–water interface. Table S2b. A comparison of the experimental conditions in studies investigating the dilational rheology of adsorbed BSA films at an air–water interface. Table S2c. A comparison of the experimental conditions in studies investigating the dilational rheology of adsorbed HSA films at an air–water interface. Table S2d. A comparison of the experimental conditions in studies investigating the dilational rheology of adsorbed LYS films at an air–water interface. Table S2e. A comparison of the experimental conditions in studies investigating the dilational rheology of adsorbed OVA films at an air–water interface. Table S3. A comparison of  $t_{life}$  amongst studies [42–61] investigating adsorbed globular protein films at an air–water interface. Table S4. Data pertaining to perturbances ( $p_7$ ,  $p_i$ – $p_{iii}$ ) in Figure 2a, Figures S3 and S4. Table S5. Data pertaining to the perturbances ①–③ in Figure S12. Figure S1. (a) Relaxations of surface tension ( $\gamma$ ) and surface area ( $A$ ) of purely aqueous BSA solution ( $C = 15 \times 10^{-10}$  mol/cm<sup>3</sup>) and the pendant bubble, respectively, showing two examples of the near-synchronized fluctuations in ST and SA at the quasi-equilibrium regime (b,c).  $P_i$  and  $Q_e$  indicate post-induction (latter) and quasi-equilibrium regimes, respectively. Figure S2. Relaxations of surface tension ( $\gamma$ ) and surface area ( $A$ ) of purely aqueous BSA solution and the pendant bubble, respectively, at  $C = 0.4$  (a,b) and  $6$  (c,d) ( $10^{-10}$  mol/cm<sup>3</sup>).  $P_e$ ,  $P_l$ , and  $Q_e$  indicate post-induction (early, latter) and quasi-equilibrium regimes, respectively. Figure S3. Relaxations of ST ( $\gamma$ ) and SA ( $A$ ) of BSA(aq) solution at  $C = 15 \times 10^{-10}$  mol/cm<sup>3</sup>, depicting a perturbation ( $p_7$ ) that was identified at the latter post-induction ( $P_l$ ) regime. Figure S4. (a) Relaxations of ST ( $\gamma$ ) and SA ( $A$ ) of BSA(aq) solution, at  $C = 15 \times 10^{-10}$  mol/cm<sup>3</sup>, showing three perturbances identified at the post-induction (b) and quasi-equilibrium (c,d) regimes. Figure S5. (a,c,e) Variation of the dilational modulus ( $E$ , ○) of an adsorbed BSA film ( $C_{BSA} = 15 \times 10^{-10}$  mol/cm<sup>3</sup>) as a function of time alongside the corresponding ST and SA relaxations. Dependency between the rate of ST change ( $d\gamma/dt$ ) and relative surface expansion rate ( $d\ln A/dt$ ) of the perturbances (○) identified  $t = 0.04\text{--}0.15$  (b,d) and  $t = 9.3\text{--}10.5$  (f) ( $10^4$  s), respectively; wherein,  $E_{avg}$  was obtained from the slope of the best-fitted line. Figure S6. Variation of  $E_{avg}$  (average dilational modulus) of the adsorbed BSA film as a function of time alongside the corresponding ST ( $\gamma$ ) and SA ( $A$ ) relaxations at  $C_{BSA} = 15 \times 10^{-10}$  mol/cm<sup>3</sup>.  $P_e$ ,  $P_l$ ,  $Q_e$  refers to the post-induction (early, latter) and quasi-equilibrium regimes. The triangle (Δ) signifies the minimum value of  $E_{avg}$ , and the plus (+) signifies the subsequent increase and oscillation. Figure S7. Variation of  $E_{avg}$  of the adsorbed BSA film as a function of time alongside the corresponding ST ( $\gamma$ ) and SA ( $A$ ) relaxations at  $C_{BSA} = 0.4$  (a) and  $6$  (b) ( $10^{-10}$  mol/cm<sup>3</sup>).  $P_e$ ,  $P_l$ ,  $Q_e$  refers to the post-induction (early, latter) and quasi-equilibrium regimes. The triangle (Δ) signifies the minimum value of  $E_{avg}$ , and the plus (+) signifies the subsequent increase and oscillation. Figure

S8. Estimated time taken for the adsorbed BSA film to reach its saturated state ( $t_{\text{sat}}$ ) at varying  $C_{\text{BSA}}$ . The horizontal bars represent the time range for earliest stable  $E_{\text{avg}}$  detected. Figure S9. Variation of  $E_{\text{avg}}$  of the adsorbed BSA film as a function of time alongside the corresponding ST ( $\gamma$ ) and SA (A) relaxations at  $C_{\text{BSA}} = 15 \times 10^{-10} \text{ mol/cm}^3$ . The vertical dashed lines indicate the  $t_{\text{sat}}$ . Figure S10. Relaxations of ST ( $\gamma$ ) and SA (A) of  $\text{BSA}_{(\text{aq})}$  (at  $C = 15 \times 10^{-10} \text{ mol/cm}^3$ ) during a rapid perturbation (compression-expansion) of the pendant bubble. Figure S11. Relaxations of ST ( $\gamma$ ) and SA (A) of  $\text{BSA}_{(\text{aq})}$  (at  $C = 0.4 \times 10^{-10} \text{ mol/cm}^3$ ) during a rapid perturbation (compression-expansion) of the pendant bubble. Figure S12. (a) Relaxations of ST ( $\gamma$ ) and SA (A) of  $\text{BSA}_{(\text{aq})}$ , at  $C = 0.4 \times 10^{-10} \text{ mol/cm}^3$ , during a rapid perturbation (compression-expansion) of the pendant bubble and (b) the corresponding variation of  $E_{\text{avg}}$  of the adsorbed BSA film as a function of time. The labels 'a–f' signifies the  $E_{\text{avg}}$  values in Figure 4a (of the manuscript). Figure S13. Relaxations of ST ( $\gamma$ ) and SA (A) of a  $\text{BSA}_{(\text{aq})}$  solution at  $C = 15 \times 10^{-10} \text{ mol/cm}^3$ , showing the first three identifiable perturbances (①②③) at the latter post-induction regime.  $P_e$ ,  $P_l$ ,  $Q_e$  refers to the post-induction (early, latter) and quasi-equilibrium regimes. Figure S14. (a) Variation of  $E_{\text{avg}}$  of the adsorbed BSA film ( $C_{\text{BSA}} = 15 \times 10^{-10} \text{ mol/cm}^3$ ) as a function of time alongside the corresponding ST ( $\gamma$ ) and SA (A) relaxations. (b–d) Dependency between the rate of ST change ( $d\gamma/dt$ ) and relative surface expansion rate ( $d\ln A/dt$ ) of the perturbances (○) identified at  $t = 130$ – $330 \text{ s}$ ; wherein,  $E_{\text{avg}}$  was obtained from the slope of the best-fitted line. Figure S15. (a) Variation of  $E_{\text{avg}}$  of the adsorbed BSA film ( $C_{\text{BSA}} = 15 \times 10^{-10} \text{ mol/cm}^3$ ) as a function of time alongside the corresponding ST ( $\gamma$ ) and SA (A) relaxations. (b–f) Dependency between the rate of ST change ( $d\gamma/dt$ ) and relative surface expansion rate ( $d\ln A/dt$ ) of those perturbances (○) identified at  $t = 0.01$ – $4.5 (10^4 \text{ s})$ ; wherein,  $E_{\text{avg}}$  was obtained from the slope of the best-fitted line.  $P_l$  and  $Q_e$  labels refer to the post-induction (latter) and quasi-equilibrium regimes. Figure S16. (a,b) Variation of  $E_{\text{avg}}$  of the adsorbed BSA film ( $C_{\text{BSA}} = 6 \times 10^{-10} \text{ mol/cm}^3$ ) as a function of time alongside the corresponding ST ( $\gamma$ ) and SA (A) relaxations. (c–l) Dependency between the rate of ST change ( $d\gamma/dt$ ) and relative surface expansion rate ( $d\ln A/dt$ ) of the perturbances (○) identified at  $t = 0.03$ – $2.0 (10^4 \text{ s})$ ; wherein,  $E_{\text{avg}}$  was obtained from the slope of the best-fitted line. The labels  $P_e$ ,  $P_l$ , and  $Q_e$  refer to the post-induction (early and latter) and the quasi-equilibrium regimes.

**Author Contributions:** Conceptualization, W.-C.T., R.-Y.T., G.L., B.N. and S.-Y.L.; Methodology, W.-C.T., R.-Y.T. and S.-Y.L.; Software, S.H. and J.E.M.R.; Validation, W.-C.T., R.-Y.T., B.N. and S.-Y.L.; Formal analysis, S.H., J.E.M.R. and S.-Y.L.; Investigation, S.H., J.E.M.R. and S.-Y.L.; Data curation, S.H. and J.E.M.R.; Writing—original draft preparation, S.H. and S.-Y.L.; Writing—review and editing, S.H. and S.-Y.L.; Visualization, S.H.; Supervision, S.-Y.L.; Project administration, S.-Y.L., G.L. and B.N.; Funding acquisition, S.-Y.L. All authors have read and agreed to the published version of the manuscript. All authors have read and agreed to the published version of the manuscript

**Funding:** The authors take this opportunity to acknowledge the financial support from the Ministry of Science and Technology, Taiwan (Project No: MOST 109-2221-E-011-055-MY3 and MOST 108-2923-E-011-004-MY3).

**Data Availability Statement:** The data presented in this study are available on request from the corresponding author.

**Acknowledgments:** The authors extend a token of gratitude to Tran Van Nho for his assistance with the experiments.

**Conflicts of Interest:** The authors declare no conflicts of interest. The funders had no role in the design of the study; in the collection, analyses, or interpretation of data; in the writing of the manuscript; or in the decision to publish the results.

## References

1. Ashoorirad, M.; Fallah, A.; Saviz, M. Measuring and assessment of impedance spectrum of collagen thin films in the presence of deionized water. *J. Mol. Liq.* **2020**, *320*, 114488.
2. Gebauer, M.; Skerra, A. Engineered Protein Scaffolds as Next-Generation Therapeutics. *Annu. Rev. Pharmacol. Toxicol.* **2020**, *60*, 391–415.
3. Ferreira, R.R.; Souza, A.G.; Rosa, D.S. Essential oil-loaded nanocapsules and their application on PBAT biodegradable films. *J. Mol. Liq.* **2021**, *337*, 116488.
4. Calva-Estrada, S.J.; Jiménez-Fernández, M.; Lugo-Cervantes, E. Protein-Based Films: Advances in the Development of Bio-materials Applicable to Food Packaging. *Food Eng. Rev.* **2019**, *11*, 78–92.
5. Galani, E.; Ly, I.; Laurichesse, E.; Schmitt, V.; Xenakis, A.; Chatzidaki, M.D. Pea and Soy Protein Stabilized Emulsions: Formulation, Structure, and Stability Studies. *Colloids Interfaces* **2023**, *7*, 30.

6. Jaganathan, M.; Selvaraju, C.; Dhathathreyan, A. pH induced reorganization of protein-protein interface in liposome encapsulated Ferritin at air/fluid and fluid/solid interfaces. *J. Mol. Liq.* **2020**, *312*, 113422.
7. Zottig, X.; Côté-Cyr, M.; Arpin, D.; Archambault, D.; Bourgault, S. Protein Supramolecular Structures: From Self-Assembly to Nanovaccine Design. *Nanomaterials* **2020**, *10*, 1008.
8. Chen, B.; Wang, H.; Zhang, H.; He, Z.; Zhang, S.; Liu, T.; Zhou, Y. A novel hydrogen peroxide sensor based on hemoglobin immobilized PAN-SiO<sub>2</sub>/DTAB composite film. *J. Mol. Liq.* **2012**, *171*, 23–28.
9. Quijano-Rubio, A.; Yeh, H.W.; Park, J.; Lee, H.; Langan, R.A.; Boyken, S.E.; Lajoie, M.J.; Cao, L.; Chow, C.M.; Miranda, M.C.; et al. De novo design of modular and tunable protein biosensors. *Nature* **2021**, *591*, 482–487.
10. Chen, Y.; Nai, X.; Li, M.; Kong, J.; Hao, S.; Yan, H.; Liu, M.; Zhang, Q.; Liu, J. A comprehensive research on Lactone Sophorolipid (LSL) and Soy Protein Isolate (SPI) interacting mixture. *J. Mol. Liq.* **2021**, *339*, 117239.
11. Wagoner, T.; Vardhanabhati, B.; Foegeding, E.A. Designing Whey Protein–Polysaccharide Particles for Colloidal Stability. *Annu. Rev. Food Sci. Technol.* **2016**, *7*, 93–116.
12. Sarigiannidou, K.; Odelli, D.; Jessen, F.; Mohammadifar, M.A.; Ajalloueian, F.; Vall-Llosera, M.; de Carvalho, A.F.; Casanova, F. Interfacial Properties of Pea Protein Hydrolysate: The Effect of Ionic Strength. *Colloids Interfaces* **2022**, *6*, 76.
13. Bhowal, A.C.; Kundu, S. Time dependent gold nanoclusters and nanocrystals formation on BSA at solid-water and air-solid interfaces. *J. Mol. Liq.* **2016**, *224*, 89–94.
14. Atkinson, P.J.; Dickinson, E.; Horne, D.S.; Richardson, R.M. Neutron reflectivity of adsorbed  $\beta$ -casein and  $\beta$ -lactoglobulin at the air/water interface. *J. Chem. Soc. Faraday Trans.* **1995**, *91*, 2847–2854.
15. Dickinson, E. Adsorbed protein layers at fluid interfaces: Interactions, structure and surface rheology. *Colloids Surf. B Biointerfaces* **1999**, *15*, 161–176.
16. Renault, A.; Pezenec, S.; Gauthier, F.; Vié, V.; Desbat, B. Surface Rheological Properties of Native and S-Ovalbumin Are Correlated with the Development of an Intermolecular  $\beta$ -Sheet Network at the Air–Water Interface. *Langmuir* **2002**, *18*, 6887–6895.
17. Postel, C.; Abillon, O.; Desbat, B. Structure and denaturation of adsorbed lysozyme at the air–water interface. *J. Colloid Interface Sci.* **2003**, *266*, 74–81.
18. Martin, A.H.; Stuart, M.A.C.; Bos, M.A.; van Vliet, T. Correlation between Mechanical Behavior of Protein Films at the Air/Water Interface and Intrinsic Stability of Protein Molecules. *Langmuir* **2005**, *21*, 4083–4089.
19. Mitropoulos, V.; Mütze, A.; Fischer, P. Mechanical properties of protein adsorption layers at the air/water and oil/water interface: A comparison in light of the thermodynamical stability of proteins. *Adv. Colloid Interface Sci.* **2014**, *206*, 195–206.
20. Strazdaite, S.; Navakauskas, E.; Kirschner, J.; Sneideris, T.; Niaura, G. Structure Determination of Hen Egg-White Lysozyme Aggregates Adsorbed to Lipid/Water and Air/Water Interfaces. *Langmuir* **2020**, *36*, 4766–4775.
21. Ravera, F.; Dziza, K.; Santini, E.; Cristofolini, L.; Liggieri, L. Emulsification and emulsion stability: The role of the interfacial properties. *Adv. Colloid Interface Sci.* **2021**, *288*, 102344.
22. Sun, H.Q.; Zhang, L.; Li, Z.Q.; Zhang, L.; Luo, L.; Zhao, S. Interfacial dilational rheology related to enhance oil recovery. *Soft Matter* **2011**, *7*, 7601.
23. Lin, S.; McKeigue, K.; Maldarelli, C. Diffusion-controlled surfactant adsorption studied by pendant drop digitization. *AIChE J.* **1990**, *36*, 1785–1795.
24. Hussain, S.; Le, T.T.Y.; Tsay, R.-Y.; Lin, S.-Y. Solubility determination of surface-active components from dynamic surface tension data. *J. Ind. Eng. Chem.* **2020**, *92*, 297–302.
25. Lin, S.Y.; Hwang, H.F. Measurement of Low Interfacial Tension by Pendant Drop Digitization. *Langmuir* **1994**, *10*, 4703–4709.
26. Tseng, W.C.; Tsay, R.Y.; Le, T.T.Y.; Hussain, S.; Noskov, B.A.; Akentiev, A.; Yeh, H.H.; Lin, S.Y. Evaluation of the dilational modulus of protein films by pendant bubble tensiometry. *J. Mol. Liq.* **2022**, *349*, 118113.
27. Beverung, C.; Radke, C.J.; Blanch, H.W. Protein adsorption at the oil/water interface: Characterization of adsorption kinetics by dynamic interfacial tension measurements. *Biophys. Chem.* **1999**, *81*, 59–80.
28. Lucassen, J. Dynamic dilational properties of composite surfaces. *Colloids Surfaces* **1992**, *65*, 139–149.
29. Walstra, P. *Physical Chemistry of Foods*; CRC Press: Boca Raton, FL, USA, 2002.
30. Roberts, S.A.; Kellaway, I.W.; Taylor, K.M.G.; Warburton, B.; Peters, K. Combined Surface Pressure–Interfacial Shear Rheology Study of the Effect of pH on the Adsorption of Proteins at the Air–Water Interface. *Langmuir* **2005**, *21*, 7342–7348.
31. Wang, H.Y. Influence of Oleic Acid and Electrolyte on the Interfacial Dilational Properties of Surfactant/Polymer Systems at the Decane–Water Interface. *J. Dispers. Sci. Technol.* **2010**, *31*, 1658–1666.
32. Hunter, J.R.; Kilpatrick, P.K.; Carbonell, R.G. Lysozyme adsorption at the air/water interface. *J. Colloid Interface Sci.* **1990**, *137*, 462–482.
33. Cornec, M.; Narsimhan, G. Adsorption and Exchange of  $\beta$ -Lactoglobulin onto Spread Monoglyceride Monolayers at the Air–Water Interface. *Langmuir* **2000**, *16*, 1216–1225.
34. Hunter, J.R.; Kilpatrick, P.K.; Carbonell, R.G.  $\beta$ -casein adsorption at the air/water interface. *J. Colloid Interface Sci.* **1991**, *142*, 429–447.
35. Poirier, A.; Banc, A.; Stocco, A.; In, M.; Ramos, L. Multistep building of a soft plant protein film at the air-water interface. *J. Colloid Interface Sci.* **2018**, *526*, 337–346.
36. Damodaran, S.; Xu, S. The Role of Electrostatic Forces in Anomalous Adsorption Behavior of Phosvitin at the Air/Water Interface. *J. Colloid Interface Sci.* **1996**, *178*, 426–435.

37. Narsimhan, G.; Uraizee, F. Kinetics of Adsorption of Globular Proteins at an Air–Water Interface. *Biotechnol. Prog.* **1992**, *8*, 187–196.
38. Le, T.T.Y.; Hussain, S.; Tsay, R.Y.; Lin, S.Y. On the adsorption kinetics of bovine serum albumin at the air–water interface. *J. Mol. Liq.* **2022**, *353*, 118813.
39. Muñoz, M.G.; Monroy, F.; Ortega, F.; Rubio, R.G.; Langevin, D. Monolayers of Symmetric Triblock Copolymers at the Air–Water Interface. 2. Adsorption Kinetics. *Langmuir* **2000**, *16*, 1094–1101.
40. Rivillon, S.; Muñoz, M.G.; Monroy, F.; Ortega, F.; Rubio, R.G. Experimental Study of the Dynamic Properties of Monolayers of PS–PEO Block Copolymers: The Attractive Monomer Surface Case. *Macromolecules* **2003**, *36*, 4068–4077.
41. Llamas, S.; Mendoza, A.J.; Guzmán, E.; Ortega, F.; Rubio, R.G. Salt effects on the air/solution interfacial properties of PEO-containing copolymers: Equilibrium, adsorption kinetics and surface rheological behavior. *J. Colloid Interface Sci.* **2013**, *400*, 49–58.
42. Benjamins, J.; Lucassen-Reynders, E.H. Surface dilational rheology of proteins adsorbed at air/water and oil/water interfaces. In *Proteins at Liquid Interfaces*; Mobius, D., Miller, R., Eds.; Elsevier: Amsterdam, The Netherlands, 1998; pp. 341–384.
43. Pereira, L.G.C.; Théodoly, O.; Blanch, H.W.; Radke, C.J. Dilatational Rheology of BSA Conformers at the Air/Water Interface. *Langmuir* **2003**, *19*, 2349–2356, <https://doi.org/10.1021/la020720e>.
44. Berthold, A.; Schubert, H.; Brandes, N.; Kroh, L.; Miller, R. Behaviour of BSA and of BSA-derivatives at the air/water interface. *Colloids Surfaces A: Physicochem. Eng. Asp.* **2007**, *301*, 16–22, <https://doi.org/10.1016/j.colsurfa.2006.11.054>.
45. Noskov, B.A.; Mikhailovskaya, A.A.; Lin, S.-Y.; Loglio, G.; Miller, R. Bovine Serum Albumin Unfolding at the Air/Water Interface as Studied by Dilational Surface Rheology. *Langmuir* **2010**, *26*, 17225–17231, <https://doi.org/10.1021/la103360h>.
46. Yang, J.; Yu, K.; Tsuji, T.; Jha, R.; Zuo, Y.Y. Determining the surface dilational rheology of surfactant and protein films with a droplet waveform generator. *J. Colloid Interface Sci.* **2018**, *537*, 547–553, <https://doi.org/10.1016/j.jcis.2018.11.054>.
47. Milyaeva, O.Y. Dynamic Surface Properties of Solutions of Bovine Serum Albumin Complexes with Silica Nanoparticles. *Colloid J.* **2020**, *82*, 538–545, <https://doi.org/10.1134/s1061933x20050117>.
48. Pittia, P.; Wilde, P.J.; Husband, F.A.; Clark, D.C. Functional and Structural Properties of  $\beta$ -lactoglobulin as Affected by High Pressure Treatment. *J. Food Sci.* **1996**, *61*, 1123–1128, <https://doi.org/10.1111/j.1365-2621.1996.tb10944.x>.
49. Wüstneck, R.; Moser, B.; Muschiolik, G. Interfacial dilational behaviour of adsorbed  $\beta$ -lactoglobulin layers at the different fluid interfaces. *Colloids Surfaces B: Biointerfaces* **1999**, *15*, 263–273, [https://doi.org/10.1016/s0927-7765\(99\)00093-4](https://doi.org/10.1016/s0927-7765(99)00093-4).
50. Noskov, B.A.; Grigoriev, D.O.; Latnikova, A.V.; Lin, S.-Y.; Loglio, G.; Miller, R. Impact of Globule Unfolding on Dilational Viscoelasticity of  $\beta$ -Lactoglobulin Adsorption Layers. *J. Phys. Chem. B* **2009**, *113*, 13398–13404, <https://doi.org/10.1021/jp905413q>.
51. Ulaganathan, V.; Retzlaff, I.; Won, J.Y.; Gochev, G.; Gunes, D.Z.; Gehin-Delval, C.; Leser, M.; Noskov, B.A.; Miller, R.  $\beta$ -Lactoglobulin adsorption layers at the water/air surface: 2. Dilational rheology: Effect of pH and ionic strength. *Colloids Surf. A Physicochem. Eng. Asp.* **2017**, *521*, 167–176.
52. Wierenga, P.A.; Meinders, M.B.J.; Egmond, M.R.; Voragen, A.G.J.; de Jongh, H.H.J. Quantitative Description of the Relation between Protein Net Charge and Protein Adsorption to Air–Water Interfaces. *J. Phys. Chem. B* **2005**, *109*, 16946–16952, <https://doi.org/10.1021/jp050990g>.
53. Xiong, W.; Li, J.; Li, B.; Wang, L. Physicochemical properties and interfacial dilatational rheological behavior at air–water interface of high intensity ultrasound modified ovalbumin: Effect of ionic strength. *Food Hydrocoll.* **2019**, *97*, 105210, <https://doi.org/10.1016/j.foodhyd.2019.105210>.
54. Delahaije, R.J.; Lech, F.J.; Wierenga, P.A. Investigating the effect of temperature on the formation and stabilization of ovalbumin foams. *Food Hydrocoll.* **2019**, *91*, 263–274, <https://doi.org/10.1016/j.foodhyd.2019.01.030>.
55. Delahaije, R.J.; Gruppen, H.; Giuseppin, M.L.; Wierenga, P.A. Quantitative description of the parameters affecting the adsorption behaviour of globular proteins. *Colloids Surf. B Biointerfaces* **2014**, *123*, 199–206, <https://doi.org/10.1016/j.colsurfb.2014.09.015>.
56. Milyaeva, O.Y.; Campbell, R.A.; Lin, S.-Y.; Loglio, G.; Miller, R.; Tihonov, M.M.; Varga, I.; Volkova, A.V.; Noskov, B.A. Synergetic effect of sodium polystyrene sulfonate and guanidine hydrochloride on the surface properties of lysozyme solutions. *RSC Adv.* **2014**, *5*, 7413–7422, <https://doi.org/10.1039/c4ra14330b>.
57. Tihonov, M.; Milyaeva, O.; Noskov, B. Dynamic surface properties of lysozyme solutions. Impact of urea and guanidine hydrochloride. *Colloids Surf. B Biointerfaces* **2015**, *129*, 114–120, <https://doi.org/10.1016/j.colsurfb.2015.03.034>.
58. Bénarouche, A.; Habchi, J.; Cagna, A.; Maniti, O.; Girard-Egrot, A.; Cavalier, J.F.; Longhi, S.; Carrière, F. Interfacial properties of NTA1L, an intrinsically disordered protein. *Biophys. J.* **2017**, *113*, 2723–2735.
59. Miller, R.; Fainerman, V.; Makievski, A.; Krägel, J.; Grigoriev, D.; Kazakov, V.; Sinyachenko, O. Dynamics of protein and mixed protein/surfactant adsorption layers at the water/fluid interface. *Adv. Colloid Interface Sci.* **2000**, *86*, 39–82, [https://doi.org/10.1016/s0001-8686\(00\)00032-4](https://doi.org/10.1016/s0001-8686(00)00032-4).

60. Fainerman, V.B.; Kovalchuk, V.I.; Aksenenko, E.V.; Zinkovych, I.I.; Makievski, A.V.; Nikolenko, M.V.; Miller, R. Dilational Viscoelasticity of Proteins Solutions in Dynamic Conditions. *Langmuir* **2018**, *34*, 6678–6686, <https://doi.org/10.1021/acs.langmuir.8b00631>.
61. Kovalchuk, V.I.; Aksenenko, E.V.; Trukhin, D.V.; Makievski, A.V.; Fainerman, V.B.; Miller, R. Effect of Amplitude on the Surface Dilational Visco-Elasticity of Protein Solutions. *Colloids Interfaces* **2018**, *2*, 57, <https://doi.org/10.3390/colloids2040057>.

**Disclaimer/Publisher's Note:** The statements, opinions and data contained in all publications are solely those of the individual author(s) and contributor(s) and not of MDPI and/or the editor(s). MDPI and/or the editor(s) disclaim responsibility for any injury to people or property resulting from any ideas, methods, instructions or products referred to in the content.